

Exploring the effect of material and geometric coupling on friction and energy dissipation in rough contacts of soft coatings

N. Menga,^{1,2,*} G. Carbone,^{1,2} and D. Dini²

¹*Department of Mechanics, Mathematics and Management,
Politecnico of Bari, V.le Japigia, 182, 70126, Bari, Italy*

²*Imperial College London, Department of Mechanical Engineering,
Exhibition Road, London SW7 2AZ*

Abstract

We study the frictional behavior of both elastic and viscoelastic thin coatings in sliding rough contact in the presence of Coulomb friction at the interface, exploring the effect of the coupling between the normal and tangential displacement fields arising from the finiteness of the material thickness.

We found that due to this so called *geometric* coupling asymmetric contacts and consequently keying friction are observed even for purely elastic contacts, indeed associated with zero bulk energy dissipation. Furthermore, enhanced keying friction is reported in the case of viscoelastic coatings compared to uncoupled contacts, this time entailing larger bulk energy dissipation.

Geometric coupling also introduces additional interactions involving the larger scales in terms of normal displacements, which leads to a significant increase of the contact area, under given normal load, compared to the uncoupled case.

These results show that, in the case of contact interfaces involving thin deformable coating bonded to significantly stiffer substrate, the effect of interfacial shear stresses cannot be neglected.

Keywords: roughness, contact mechanics, friction, coating, shear stress, coupling

*Electronic address: nicola.menga@poliba.it

I. INTRODUCTION

Nowadays, a large number of systems in several application fields involve layered materials. Soft coatings are one of the most frequent examples of such cases, with a thin film with specific characteristics deposited onto a substrate in order to tailor the overall system behavior (e.g. chemical resistance to corrosion, enhanced or reduced stiffness, damping, frictional behavior). They are widely used, for instance, in engines where specific low friction coatings are adopted to reduce energy dissipation (and, in turn, heat generation) in key contacting pairs, such as valve train systems and crankshafts [1, 2]. At the same time, high frictional coatings are also required to increase the grip of stiff substrates in applications including robotic clamps for objects manipulation [3] or anti-skid tapes to prevent slip on ramps and stairs. Coatings are also present in the case of biological systems such as human hands and feet, where the covering skin (which may locally be constituted by very thin layers) concurs in developing the high interfacial friction sustaining, for instance, the firm hand grip on the tennis racket handle, or the barefoot walking on different grounds.

For these reasons, a constantly rising interest on the tribological behavior of thin coatings has been reported in the last decades. Indeed, besides the theoretical [4–11], numerical [12–17] and experimental [18–21] studies focusing on contact problems where both bodies can be treated as half-spaces (or semi-infinite), detailed investigations have been also devoted to the case of interfaces involving thin bodies [22–26] leading to qualitatively different results with respect to half-space solutions.

In the presence of thin deformable contacting bodies, tangential interactions are strongly coupled to the local deformations of the system, which are not accommodated remotely as is the case when the half-space approximation is invoked. In a recent work [27] it has been shown that, dealing with contacts of thin soft layers, the interfacial tangential stress strongly affects the tribological interface behavior, both in terms of contact area and gap distribution. This is because two possible independent sources of interaction exist between the normal and tangential elastic fields in thin films: (i) the "material" coupling, vanishing in the case of incompressible or similar materials between the contacting pair elements; and (ii) the "geometric" coupling, which is a thickness modulated term, vanishing for sufficiently thick coatings. The effect of the first term (i.e. the material coupling) has been explored in some studies, mostly focusing on stick-slip fretting problems associated to homogeneous [28–30] and graded [31, 32] elastic materials. Interestingly, in [28] it was reported that, in the case of dissimilar cylinders contacts, a non-negligible influence of the material coupling occurs on both the normal stiffness of the contact and the contact pressure distribution. Less effort has been made to investigate the second term (i.e. the geometric coupling), arising only for thin coatings. Indeed, moving from the pioneeristic study of Bentall and Johnson [33], only a few authors have approached the problem [34–36], and only focusing on smooth contacts and the single asperity case. The first comprehensive investigation of rough elastic contacts in the presence of geometric coupling has been provided in Ref. [27], showing that, even in the case of incompressible materials, the coupling may lead to a significant increase of the effective contact area, thus impacting on different contact-related phenomena such as interfacial hydraulic impedance, electrical conductivity [37], and wear process evolution [38].

Interestingly, the geometric coupling effects highlighted in Ref. [27] could play an even more dramatic role when dealing with the frictional performance of interfaces in relative motion. The contact asymmetry generated at the interface as the result of such coupling

suggests keying frictional effects even in purely elastic contacts. Moreover, focusing on viscoelastic thin layers, one can reasonably expect the different distribution of the contact spots induced by the coupled normal and tangential deformation fields to affect the energy dissipation occurring due to bulk viscoelasticity and, in turn, the frictional behavior of the interface. Different contact area size and distribution lead to different excitation spectra, which are in turn related to different viscoelastic responses for given specific loading and sliding conditions. To the best of the authors knowledge, an investigation on this effect is currently missing in the specialized literature, and this work aims at filling this gap.

The focus of this study is the case of a thin coating, sufficiently softer than the underlying substrate so that the latter can be assumed as rigid, in sliding contact with a rigid profile with self-affine roughness. We focus on both cases of elastic and viscoelastic materials. In order to induce coupling, the tangential contact problem explicitly considers interfacial frictional interactions; for the first time, we investigate the explicit contribution of both material and geometric coupling on the perceived response of the coating in terms of friction and energy dissipation. As already mentioned, the system configuration studied here covers several technological applications related to the grip performance of bio-inspired or natural system for handling of objects as well as many other interesting problems, including protein-coated interfaces, paints and soft coatings for industrial use, finger tip contact with touch screens.

II. THE CONTACT PROBLEM FORMULATION

The system under investigation is shown in Figure 1, where a thin soft coating bonded to a rigid substrate is sketched. The free surface of the coating is indented by a rigid profile with periodic roughness $r(x)$. According to Fig. 1, we define h the coating thickness, λ the roughness fundamental wavelength, and V the profile sliding speed. In our formulation, we assume $V \ll c_s$ with c_s being the sound speed into the coating material; furthermore, we focus on long time observations so that steady state conditions can be reasonably assumed. In what follows, we will adopt subscript 1 and 2 referring to tangential and normal quantities, respectively. Indeed, in Fig. 1, δ_2 is the total normal displacements of the rough profile, \bar{u}_2 is the mean normal displacement of the coating surface, whereas Δ is the mean penetration of the rigid profile into the deformable coating. Note that $\delta_2 = \Delta + \bar{u}_2$.

The presence of Amonton/Coulomb friction is taken into account at the contact interface. This means that, given a generic normal contact pressure distribution $p(x)$, a corresponding tangential shear stress distribution also acts on the contacting parts in the form

$$\tau(x) = \mu_c p(x); \quad x \in \Omega, \quad (1)$$

where μ_c is the friction coefficient, and $\Omega = \bigcup_{i=1}^L [\alpha_i, \beta_i]$ is the contact domain, being α_i and β_i the unknown coordinates of i -th contact spot, with $\alpha_i < \beta_i$ and $i = 1, 2, \dots, L$, where L is the unknown number of contacts. Notably, we assume μ_c independent of the relative sliding speed.

The contact problem approach exploits the reliable formulation developed in Refs [39, 40]. Indeed, building on the linearity of the material response and exploiting the problem translational invariance, the interfacial coating displacement vector $\mathbf{v} = (v_1, v_2)$ can be linked to the stress vector $\sigma = (\tau, -p)$ by means of

$$\mathbf{v}(x) = \mathbf{u}(x) - \bar{\mathbf{u}} = \int_{\Omega} ds \Theta(x-s) \sigma(s); \quad x \in \Omega, \quad (2)$$

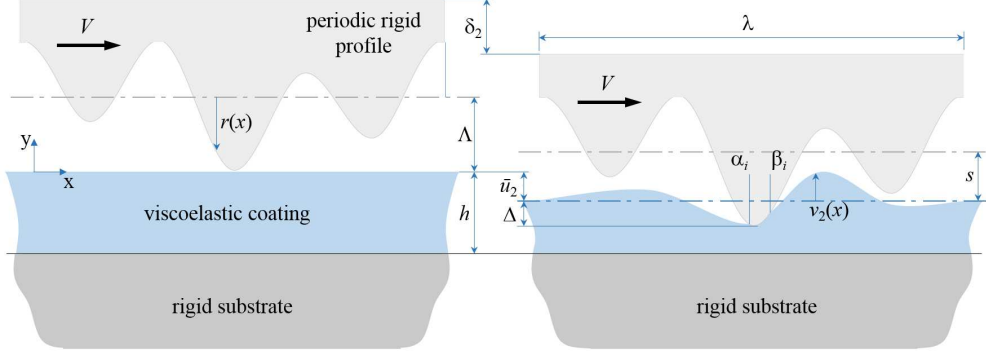


FIG. 1: A soft coating of thickness h backed onto a rigid substrate is in sliding contact with a periodic rigid profile with self-affine roughness. Coulomb friction interactions occur at the interface. The contact mean penetration is indicated with Δ , and the profile peak height is Λ .

where the time-dependency of the stress and deformation fields has been removed by invoking the coordinate transformation $x - Vt \rightarrow x$.

In Eq. (2), \mathbf{u} is the total displacement vector, and $\bar{\mathbf{u}}$ is the mean displacement vector given by

$$\bar{u}_1 = q_0 h \frac{1 + \nu}{\pi E_0} \tau_m \lambda, \quad (3)$$

$$\bar{u}_2 = q_0 h \frac{1 - 2\nu}{2\pi E_0} p_m \lambda, \quad (4)$$

where $q_0 = 2\pi/\lambda$ and E_0 is zero-frequency elastic modulus. Notably, $p_m = \frac{1}{\lambda} \int_{\Omega} p(x) dx$ and $\tau_m = \frac{1}{\lambda} \int_{\Omega} \tau(x) dx$ are the mean contact pressure and shear stress, respectively.

The term $\Theta(x) = \Theta_{kl}(x)$, with $k, l = 1, 2$ is the Green's tensor which takes different forms depending on whether the coating is elastic or viscoelastic. Indeed, in the elastic case, we have

$$\Theta_{kl}(x) = \frac{G_{kl}(x)}{E_0}, \quad (5)$$

with $G_{kl}(x)$ given by Ref. [27] as

$$G_{11}(x) = -\frac{2(1-\nu^2)}{\pi} \left[\log \left| 2 \sin \left(\frac{q_0 x}{2} \right) \right| + \sum_{m=1}^{\infty} B(mq_0 h) \frac{\cos(mq_0 x)}{m} \right], \quad (6)$$

$$G_{12}(x) = -G_{21}(x) = \frac{1+\nu}{\pi} \left[\frac{1-2\nu}{2} [\text{sgn}(x)\pi - q_0 x] - \sum_{m=1}^{\infty} C(mq_0 h) \frac{\sin(mq_0 x)}{m} \right], \quad (7)$$

$$G_{22}(x) = -\frac{2(1-\nu^2)}{\pi} \left[\log \left| 2 \sin \left(\frac{q_0 x}{2} \right) \right| + \sum_{m=1}^{\infty} A(mq_0 h) \frac{\cos(mq_0 x)}{m} \right], \quad (8)$$

with

$$A(mq_0h) = 1 + \frac{2mq_0h - (3 - 4\nu) \sinh(2mq_0h)}{5 + 2(mq_0h)^2 - 4\nu(3 - 2\nu) + (3 - 4\nu) \cosh(2mq_0h)}, \quad (9)$$

$$B(mq_0h) = 1 - \frac{2mq_0h + (3 - 4\nu) \sinh(2mq_0h)}{5 + 2(mq_0h)^2 - 4\nu(3 - 2\nu) + (3 - 4\nu) \cosh(2mq_0h)}, \quad (10)$$

$$C(mq_0h) = \frac{4(1 - \nu) [2 + (mq_0h)^2 - 6\nu + 4\nu^2]}{5 + 2(mq_0h)^2 - 4\nu(3 - 2\nu) + (3 - 4\nu) \cosh(2mq_0h)}. \quad (11)$$

On the other hand, in the case of viscoelastic coatings, extending the formulation given in Refs. [24, 40], the Green's tensor takes the form

$$\Theta_{kl}^V(x) = J(0^+) G_{kl}(x) + \int_{0^+}^{+\infty} G_{kl}(x + Vt) \dot{J}(t) dt, \quad (12)$$

which, this time, in order to take into account for the response delay in the viscoelastic material, parametrically depends on the sliding speed. In Eq. (12), the term $J(t)$ is the viscoelastic creep function, which for a linear viscoelastic material with one relaxation time τ takes the form

$$J(t) = H(t) \left[\frac{1}{E_0} - \frac{1}{E_1} \exp(-t/\tau) \right], \quad (13)$$

where $H(t)$ is the Heavyside step function, and $1/E_1 = 1/E_0 - 1/E_\infty$, with E_∞ being the high-frequency elastic modulus.

Regardless of the coating material rheology, the solution of the contact problem is found by observing that, within the contact domain Ω , the normal interfacial displacement must match the rough profile shape $r(x)$. Referring to Fig. 1, from the normal projection of Eq. (2) we have

$$r(x) - \Lambda + \Delta = \int_{\Omega} ds [\mu_c \Theta_{21}(x - s) - \Theta_{22}(x - s)] p(s); \quad x \in \Omega, \quad (14)$$

where the only unknowns are the pressure distribution $p(x)$ and the coordinates α_i, β_i corresponding to the individual contact edges. By relying on the numerical strategy based on a non-uniform contact area discretization developed in Ref. [39], for any given value of the contact penetration Δ , Eq. (14) can be numerically solved for $p(x)$, once fixed α_i, β_i . Further, the exact size of the contact area can be calculated, iteratively, by observing that, dealing with adhesiveless contact conditions, bounded contact stress are prescribed, specifically vanishing at the contact edges. Indeed, referring to Refs. [24, 40, 41] we have that

$$K_{I,\alpha_i} = - \lim_{x \rightarrow \alpha_i^+} \sqrt{2\pi(x - \alpha_i)} p(x) = 0, \quad (15)$$

$$K_{I,\beta_i} = - \lim_{x \rightarrow \beta_i^-} \sqrt{2\pi(\beta_i - x)} p(x) = 0, \quad (16)$$

where K_I is the mode I stress intensity factor.

III. RESULTS AND DISCUSSION

The presence of a deformable coating of finite thickness gives rise to an unusual coupling between the normal and tangential displacement fields. Here, we observe that in Eq. (7), beside the well-known *material* coupling term (i.e. the first right-hand side term) taking into account for the normal-tangential interactions in contact pairs of dissimilar materials (see Refs [28–30, 42]), an additional independent source of coupling (i.e. the second right-hand side term) is present, which we define as *geometric* and is a function of the coating thickness h . Notably, such a term vanishes for $h \rightarrow \infty$.

In what follows, we will investigate the role played by this *geometric* coupling on the frictional behavior of both elastic and viscoelastic interfaces, with specific focus on the interfacial and bulk energy dissipation. Furthermore, the overall contact behavior of the interface will be also investigated in the case of purely viscoelastic rubber-like coatings. Of course, this coupling is always present when the contact involves sufficiently thin layers; however, to result effective on the contact behavior a tangential stress distribution is also required. For this reason we assume frictional interfacial tractions, as for frictionless interfaces (i.e. $\mu_c \rightarrow 0$), Eqs. (2) would be completely uncoupled even for non-vanishing values of $G_{12} = -G_{21}$. Moreover, in order to highlight the qualitative differences in the overall contact behavior, the system response under frictional coupled conditions will be presented compared to frictionless uncoupled conditions.

All the calculations have been performed considering a self-affine roughness on the rigid profile. The different profile shapes have been numerically generated by exploiting the technique reported in Ref. [40]. The Power Spectral Density (PSD) $C_r(q) = (2\pi)^{-1} \int dx \langle r(0)r(x) \rangle e^{-iqx}$ of the considered roughness is given by

$$\begin{aligned} C_r(q) &= C_0 \left(\frac{|q|}{q_0} \right)^{-(2H+1)} ; & q \in [q_0, q_1] \\ C_r(q) &= 0; & q \notin [q_0, q_1] \end{aligned} \quad (17)$$

where $q_1 = Nq_0$ (being N the number of roughness scales) and H is the Hurst exponent, which is related to the fractal dimension by $D_f = 2 - H$. Profiles are generated assuming $\lambda = 6.28 \text{ mm}$, a root mean square roughness of $r_{rms} = \sqrt{\langle r^2 \rangle} = 10 \text{ }\mu\text{m}$, $H = 0.7$, and $N = 100$. In order to obtain a statistically significant contact behavior, results have been ensemble averaged on several realizations for each value of the contact parameter investigated, and are shown in terms of the following dimensionless quantities: $\tilde{h} = q_0 h$, $\tilde{a} = q_0 a$, $\tilde{\Delta} = \Delta/\Lambda$, $\tilde{v} = v/\Lambda$, $\tilde{\Lambda} = q_0 \Lambda$, $\zeta = V\tau q_0$, and $\tilde{p} = 2(1 - \nu^2)p/(E_0 q_0 \Lambda)$. In viscoelastic calculations we assume $E_\infty/E_0 = 3$.

A. Frictional behavior

In this paper we consider Coulomb friction interactions at the interface, which occurs through distributed tangential tractions at the interface, as indicated in Eq. (1). However, in the presence of asymmetric distributions of contact pressure and normal displacement, an additional term on tangential force opposing the motion arises as the tangential component of the normal pressure distribution projected along the local rough profile normal direction, which is usually referred to as keying friction. In this section we will focus on this spe-

cific friction component, investigating the effect of the normal-tangential deformation fields coupling on it.

1. Elastic contacts

Elastic rough contacts are usually not affected by mechanical keying as, dealing with semi-infinite incompressible solids in contact with rigid counterparts, no coupling occurs and symmetric pressures and displacements are expected. However, when dealing with sufficiently thin films (as well as in the case of dissimilar materials) the term $\Theta_{12} = -\Theta_{21}$ cannot be neglected in Eq. (2). Since this term is an odd function of x , its effect is to introduce a certain degree of asymmetry in the contact pressure and normal displacement distributions, although no energy dissipation occurs in the bulk material. The resulting keying frictional force F_k opposing the motion can be calculated in both the real and Fourier domain as

$$\begin{aligned} F_k &= \int_{\Omega} p(x) v_2'(x) dx \\ &= E_0 \int dq \frac{\mu_c S_{12}(|q|h)}{S_{22}^2(|q|h) + \mu_c^2 S_{12}^2(|q|h)} q^2 |v_2(q)|^2 \end{aligned} \quad (18)$$

where v_2' and $v_2(q)$ are the first spatial derivative and the Fourier transform of the normal displacement field, and $S_{11}(|q|h) = 2(1 - \nu^2)[1 - B(qh)]$, $S_{12}(|q|h) = (1 + \nu)[C(qh) - (1 - 2\nu)]$, $S_{22}(|q|h) = 2(1 - \nu^2)[1 - A(|q|h)]$. Notably, $F_k = 0$ in the case of elastic frictionless (i.e. $\mu_c = 0$) or uncoupled (i.e. semi-infinite or incompressible solids) contacts.

The total friction force F_t opposing the motion can then be written as

$$F_t = (\mu_c + \mu_k) \lambda p_m \quad (19)$$

where, according to Eqs. (18),

$$\mu_k = \frac{F_k}{\lambda p_m}. \quad (20)$$

Figures 2 show the elastic keying friction coefficient behavior in the case of elastic contacts of both compressible and incompressible materials. Compressible materials are affected by both *material* (first right-hand side term in Eq. (7)) and *geometric* coupling (second right-hand side term in Eq. (7)). However it is important to note that the two terms have opposite effects. Indeed, according to Ref. [27], dimensional arguments suggest that the correlation length of the geometric term (of order unity of h) is larger than that of the material term. This is qualitatively confirmed by the results reported in Figure 2a, where μ_k is shown against \tilde{p}_m . For $\nu = 0.3$, at very low contact pressure, where the contact spots are sufficiently small, the material coupling effect is enhanced thus, according to Eq. (7), a relief of the total friction force opposing the sliding is observed. However, as the normal load increases, larger contact spots are experienced and the geometric coupling starts playing a key role, thus increasing μ_k . For sufficiently large values of \tilde{p}_m , the geometric coupling term is dominant, thus $\mu_k > 0$ and overall increase of the total friction is expected compared to the frictionless uncoupled case. Furthermore, figure 2a shows the effect of the elastic coating thickness on μ_k . Of course, only the geometric term is affected by h , thus compressible

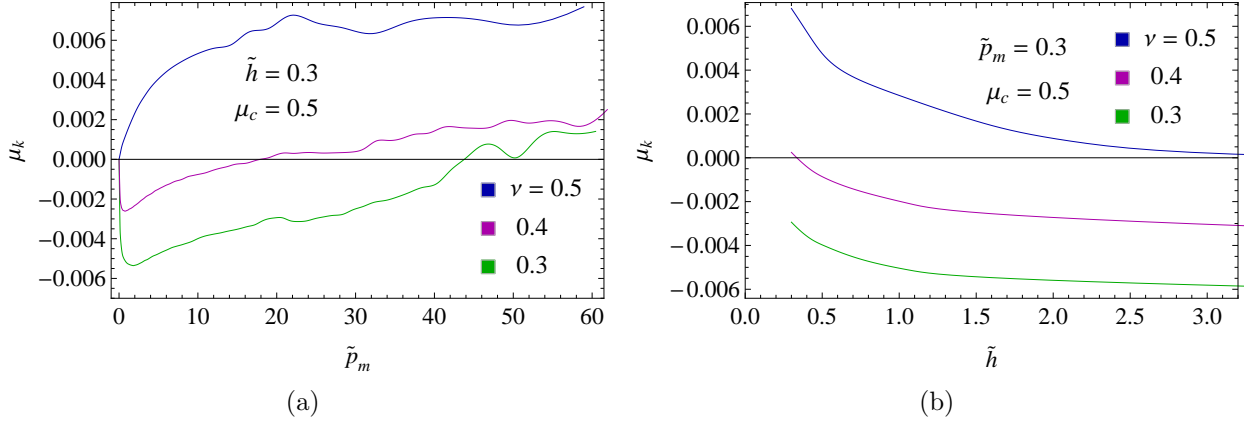


FIG. 2: The elastic keying friction coefficient μ_k as a function of (a) the dimensionless contact mean pressure \tilde{p}_m and (b) the elastic coating dimensionless thickness \tilde{h} . Results are shown for both incompressible ($\nu = 0.5$) and compressible ($\nu = 0.3$) materials.

and incompressible curves are shifted by a quantity which can be roughly estimated as the material term. Notably, for $h \rightarrow 0$ in both cases we expect $\mu_k \rightarrow 0$, as $u(q) \rightarrow 0$ in the second of Eqs. (18).

2. Viscoelastic friction

The physical picture drawn above for elastic materials is still valid in the case of viscoelastic thin coatings. However, in the presence of viscoelasticity an additional tangential load opposing the relative motion is expected due to viscous bulk energy dissipation which, even in the case of semi-infinite uncoupled solids, induces delayed material response and asymmetric normal contact pressure.

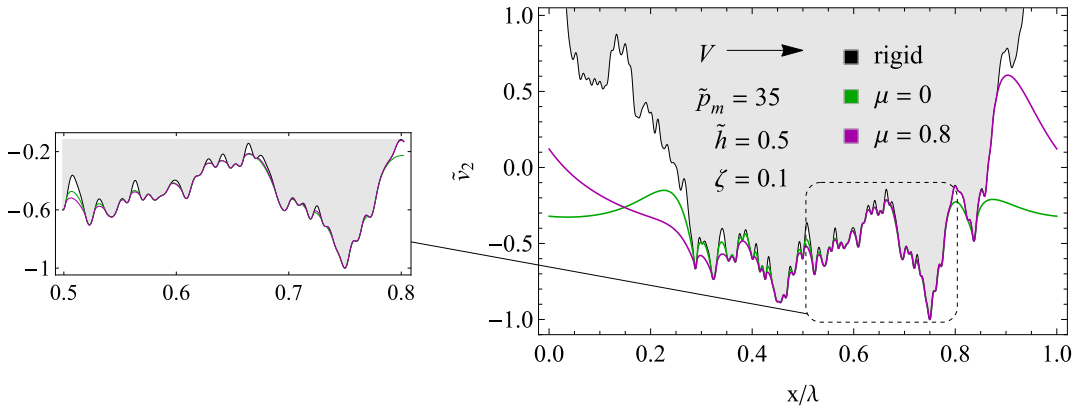


FIG. 3: The dimensionless normal displacement $v = (v + \Delta)/\Lambda - 1$, under load controlled conditions, for both the frictional coupled system and the frictionless uncoupled one in the case of viscoelastic coatings. Results are for $\nu = 0.5$.

This is clearly shown in figure 3, where the normal displacement field at the interface in both frictional coupled and frictionless uncoupled conditions is reported. In both case, a significant degree of asymmetry between the leading (right-hand side) and trailing (left-hand side) edges of each contact spots is observed. Nonetheless, in coupled conditions such a behavior is even heightened

For viscoelastic coatings, Eqs. (18) take the form

$$\begin{aligned} F_k &= \int_{\Omega} p(x) v_2'(x) dx \\ &= \int dq \tilde{E}(qV) \frac{\mu_c S_{12}(|q|h)}{S_{22}^2(|q|h) + \mu_c^2 S_{12}^2(|q|h)} q^2 |v_2(q)|^2 \end{aligned} \quad (21)$$

where, this time, $\tilde{E}(\omega) = E_0 + i\omega\tau / (1 + i\omega\tau) E_1$ is the complex viscoelastic modulus.

Furthermore, by invoking the energy balance applied to the deformable coating the bulk energy dissipation per unit time \dot{W} can be calculated as

$$\dot{W} = V \left[\int_{\Omega} p(x) v_2'(x) dx - \mu_c \int_{\Omega} p(x) v_1'(x) dx \right] \quad (22)$$

which vanishes in the case of elastic contacts.

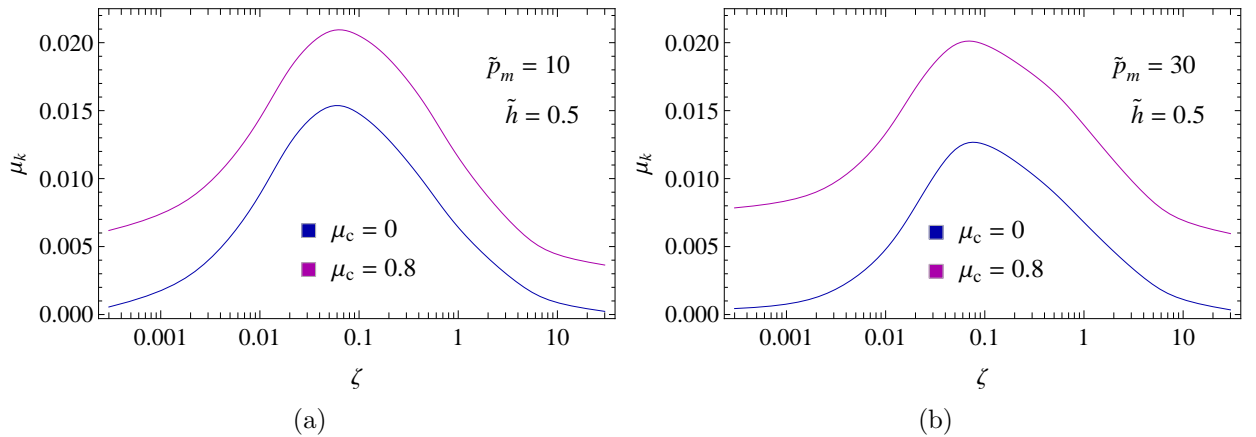


FIG. 4: The keying friction coefficient μ_k for viscoelastic coatings as a function of the dimensionless sliding speed ζ . (a) refer to the dimensionless contact mean pressure $\tilde{p}_m = 10$, and (b) to $\tilde{p}_m = 30$. Results are given for $\nu = 0.5$.

Notably, in what follows we will mostly focus on *geometric* coupling, as for most of rubber like materials $\nu \approx 0.5$. Figures 4 show the viscoelastic keying friction coefficient μ_k for both frictional coupled and frictionless uncoupled conditions as a function of the dimensionless sliding speed ζ for two different values of the dimensionless contact mean pressure. As expected, regardless on the effective amount of coupling, all the curves follow the well-known bell shaped trend, as at very low and very high sliding speed the viscoelastic material behaves elastically. Under frictional coupled conditions, generally higher keying friction is observed, as a result of additional pressure asymmetry induced by geometric

coupling. However, dealing with viscoelastic materials, the shifting factor between frictional coupled and frictionless uncoupled conditions results is still affected by the sliding speed (i.e. the excitation frequency). Furthermore, keying friction in coupled contacts appears less sensitive to the normal load variation compared to uncoupled contact conditions.

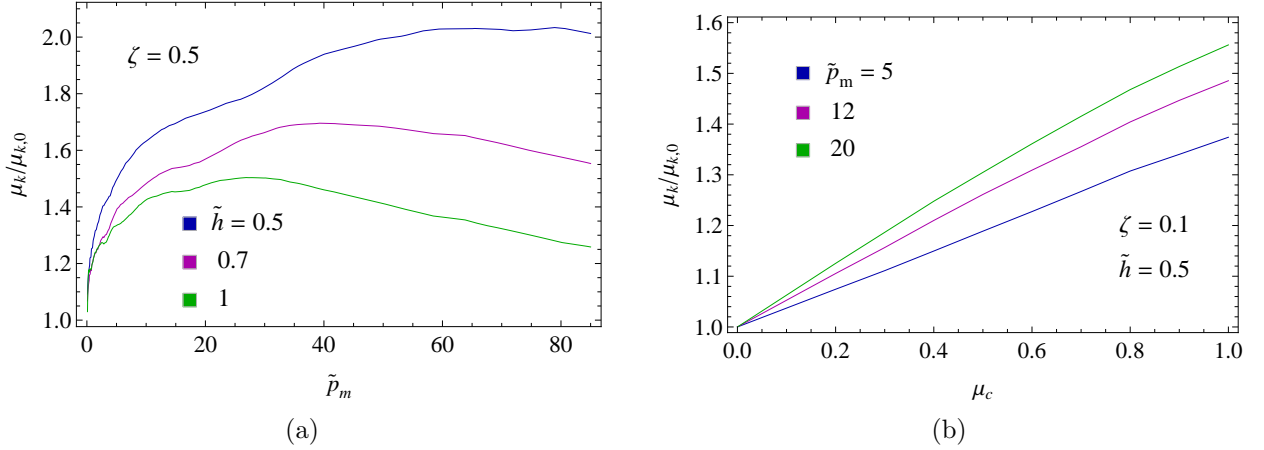


FIG. 5: The ratio $\mu_k/\mu_{k,0}$ between the viscoelastic friction coefficient in the frictional coupled and frictionless uncoupled cases, as a function of: (a) the dimensionless contact mean pressure \tilde{p}_m , for different dimensionless coating thickness \tilde{h} ; (b) the Coulombian friction coefficient μ_c , for different values of \tilde{p}_m . Results are given for $\nu = 0.5$.

In Figures 5 we show the ratio between the viscoelastic keying friction coefficient μ_k observed under frictional coupled conditions and $\mu_{k,0}$, which is the one related to the frictionless uncoupled case (i.e. only related to viscoelastic hysteresis). Specifically, in Fig. 5a, the effect of \tilde{p}_m is investigated for three different values of \tilde{h} . Of course, according to Eqs. (7-11) thinner coatings lead to higher degrees of *geometric* coupling. At very large pressures, the value of μ_k reduces as coupled systems exhibit smaller full contact pressure compared to the uncoupled ones, and further increases of p_m have slighter effects on μ_k . In Fig. 5b the effect of the Coulombian interfacial friction coefficient μ_c on μ_k is instead explored at relatively low contact mean pressures. As expected, increasing μ_c exacerbates the effects of the coupling between the normal and tangential fields increasing the interfacial shear stress, thus leading to larger values of μ_k . Nonetheless, depending on the specific value of p_m , a saturation of the phenomenon is also expected.

Figure 6 investigates the bulk energy dissipation in viscoelastic coatings. In the presence of Coulomb interfacial friction, increased bulk energy dissipation is observed as, this time, also the tangential deformations contribute to the viscoelastic dissipation. Interestingly, since the energy dissipated is converted into bulk heat, such a peculiar behavior of coupled frictional systems may be relevant when aiming at controlling the material warming. It is, for instance, the case of tyres in which a key component is the tread (a thin coating on the underlying stiffer substrate) whose warming is crucial for the overall system performance.

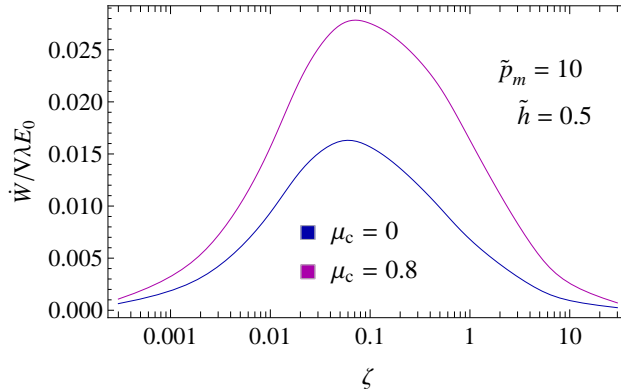


FIG. 6: The dimensionless bulk energy dissipation $\dot{W}/V\lambda E_0$ in viscoelastic thin coatings as a function of the dimensionless sliding speed ζ . Results are given for $\nu = 0.5$.

B. Viscoelastic mean contact quantities

A detailed analysis of Figure 3 reveals that a significant differences can be observed between the two conditions investigated as, given the same value of the dimensionless contact mean pressure \tilde{p}_m , both contact penetration and contact area experienced in the frictional coupled case are larger than those reported for the frictionless uncoupled one. However, by looking at the close up, we conclude that the main difference in the deformation occurs at the large spatial scales, as the behavior at the small scales appears much more similar among the two cases.

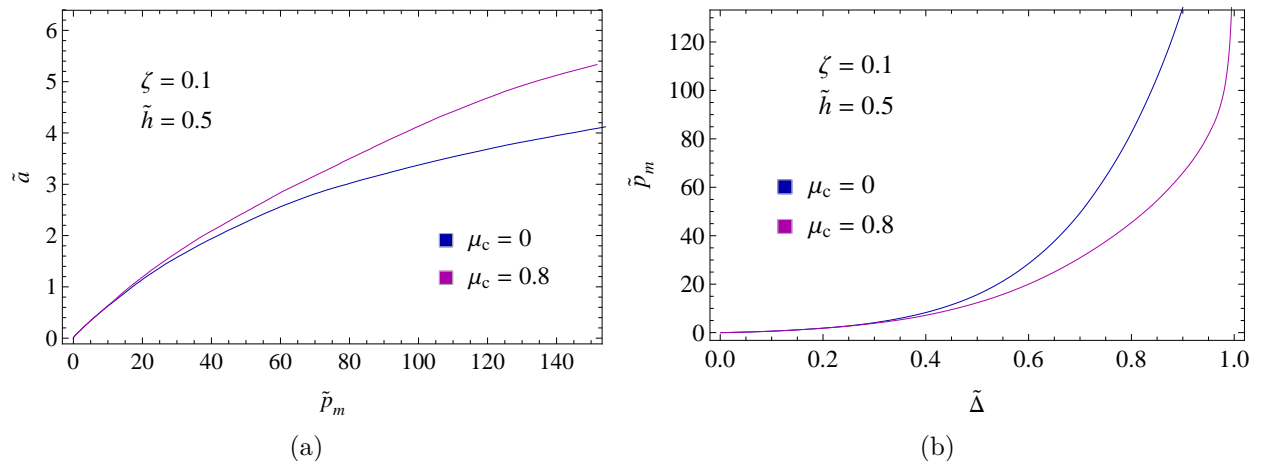


FIG. 7: The dimensionless contact area \tilde{a} as a function of the dimensionless contact mean pressure \tilde{p}_m (a); and the dimensionless contact mean pressure \tilde{p}_m as a function of the dimensionless contact penetration $\tilde{\Delta}$. Full contact is for $\tilde{a} = 2\pi$.

A more quantitative comparison is provided in Figures 7a,7b, where we show the relationship between the main contact quantities. Interestingly, from both the figures it can be

noted that the differences in the behavior of the two conditions (i.e. coupled and uncoupled) increases with \tilde{p}_m increasing. This can be explained by observing that, from Eq. (1), the shear stresses are proportional to the normal pressure, thus, at low values of \tilde{p}_m the system behaves almost frictionless thus resulting in a poor degree of coupling; whereas, increasing \tilde{p}_m leads to higher shear stresses and, in turn, to larger coupling effects. This result is in agreement with what reported in Ref. [27] for elastic coupled contacts. In the next sections, more precise inferences will be provided regarding the normal contact stiffness behavior.

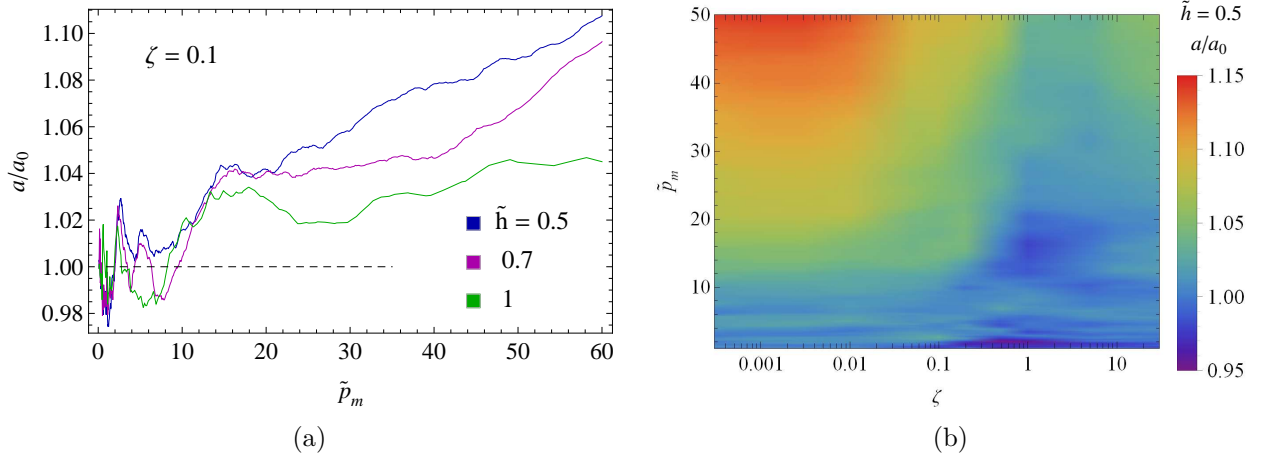


FIG. 8: The ratio between the contact area a of the frictional coupled system and that of the frictionless uncoupled one (a_0) as a function of: (a) the dimensionless contact mean pressure \tilde{p}_m for different values of the dimensionless layer thickness \tilde{h} ; (b) the dimensionless contact mean pressure \tilde{p}_m and the dimensionless sliding speed ζ . For the frictional coupled case, the friction coefficient is $\mu_c = 0.8$.

Figure 8a shows the ratio a/a_0 between the contact area in the two conditions (with a_0 being the frictionless uncoupled contact length) as a function of \tilde{p}_m , for different values of the dimensionless coating thickness \tilde{h} . At low values of the contact mean pressure, the noise in the data is mostly due to fact that the whole load is sustained only by very small contact spots, mostly localized on top of the roughness crests. This dramatically affects the statistical sampling of the rough profiles, thus leading to significant scattering in the results. However, we can still observe that, for $\tilde{p}_m \lesssim 10$, since the frictional shear stress is low, the contact interface does not experience a significant deviation from the contact area expected in uncoupled frictionless conditions, regardless of the value of \tilde{h} . On the contrary, for $\tilde{p}_m \gtrsim 10$, the coupled tangential problem starts to play a gradually increasing role on the overall contact behavior. In this condition, the component of the normal displacement coupled to the shear stress, through Eq. (7), modifies the shape of the deformed coating surface leading to a marked increase of the contact area compared to the uncoupled frictionless case. As expected, increasing the coating thickness flattens the ratio a/a_0 towards the unity value, as from Eqs. (7,11) we obtain that the "geometric" coupling effects monotonically decrease with \tilde{h} increasing, eventually leading, for $\tilde{h} \gtrsim 10$, to negligible effects (see also Ref. [27, 40]).

Figure 8b shows a contour map of the ratio a/a_0 , for a specific value of \tilde{h} , as a function of both the dimensionless sliding speed ζ and \tilde{p}_m . Interestingly, we observe that at slow sliding

speed the ratio a/a_0 is mainly higher than that reported at high sliding speed. However, such a trend is non-monotonic, as, for any given contact mean pressure, at $\zeta \approx 1$ a minimum of a/a_0 is present, whose value depends on \tilde{p}_m , according to Fig. 8a. A quantitative analysis of the data reported in Fig. 8b offers interesting perspectives, as contact length enhancements up to 15% are reported due to the geometric coupling. Such a huge difference suggests that in applications involving the contact of thin coated soft viscoelastic components, such as for instance accurate detection of finger prints on touch screens, the underestimation of the real contact area under frictional sliding provided by uncoupled models may affect the overall device functionality. On the contrary, the adoption of models able to take into account for the effect of coupled normal and tangential deformation fields on the overall contact response of the interface may propel further developments of these devices.

C. Normal displacement field

Figure 3 clearly shows that the normal displacement field is strongly affected by the *geometric* coupling. Indeed, out of the contact zone, very different normal deformations can be observed depending on whether coupled or uncoupled deformation fields (i.e. frictional or friction less conditions) are considered.

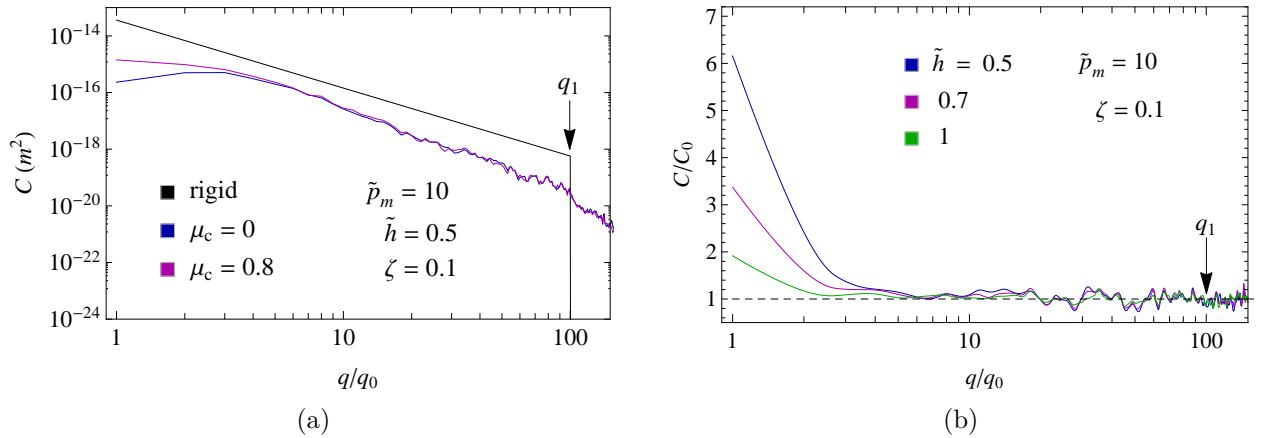


FIG. 9: The Power Spectral Density (PSD) C of the frictional coupled system compared to that (C_0) of the frictionless uncoupled one (a); the PSD ratio C/C_0 for different coating dimensionless thickness \tilde{h} . For the frictional coupled case, the friction coefficient is $\mu_c = 0.8$.

In this regard, Figure 9a offers a quantitative comparison between the Power Spectral Density (PSD) $C(q)$ of the deformed profiles under frictional coupled and frictionless uncoupled conditions. The rigid rough profile PSD is also shown to help the comparison. Results seem to indicate, under load controlled conditions, the tendency of the coupled contact interface to preferably arrange the deformation over larger scales (i.e. at lower spatial frequencies q) compared to frictionless uncoupled case. Such a result is even more clearly shown in Fig. 9b, where we plot the ratio C/C_0 between the deformed profile PSD for the frictional coupled case and that for the frictionless uncoupled one. According to Eqs. (7,11), the thinner the coating, the larger the difference in the behavior, which shows larger deformation

associated to the larger scales. At the smaller scales (i.e. for $\lambda_i = 2\pi/q \ll h$) the contact behavior recovers the one expected in the case of half-space contacts, thus neglecting any coupling between the normal and tangential displacement fields regardless of the friction intensity. Indeed, building on dimensional arguments, we expect that for $q/q_0 > \rho/\tilde{h}$, with ρ being a constant of order unity, the coupling effect should vanish. This is actually reported in Fig. 9b as the spatial frequency q at which the coupling effects vanish increases with \tilde{h} decreasing.

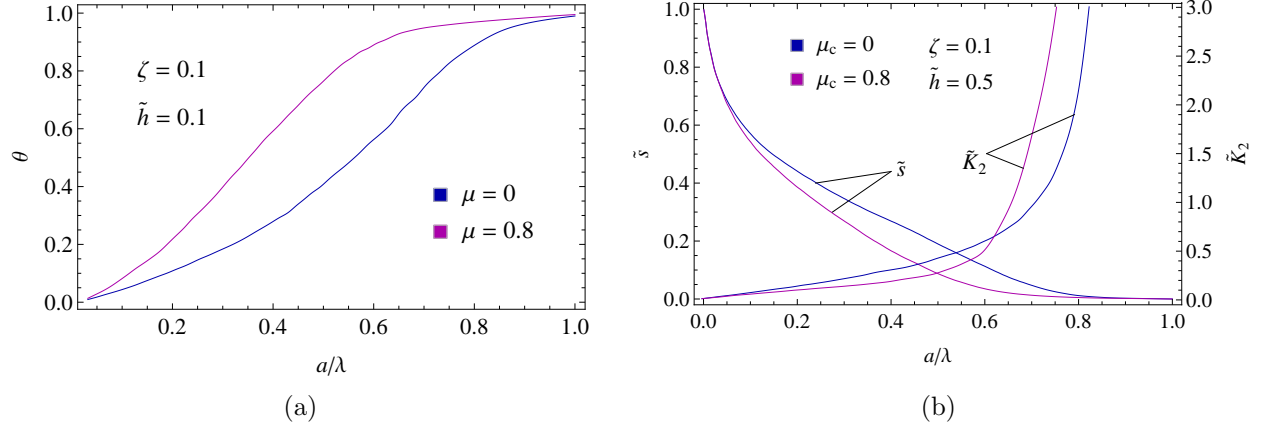


FIG. 10: The ratio θ between the frictional coupled and frictionless uncoupled systems mean square heights of the deformed profiles (a), and the dimensionless contact mean separation $\tilde{s} = s/\Lambda$ and the dimensionless normal stiffness $\tilde{K}_2 = 10^{-3}d\tilde{p}_m/d\tilde{\Delta}$ as a function of the contact area fraction a/λ . For the frictional coupled case, the friction coefficient is $\mu_c = 0.8$.

The effect of the *geometric* coupling on the spectrum of the coating normal displacement field can be further explored by defining θ as the ratio between the mean square roughness of the deformed profile and the rigid one, i.e.

$$\theta = \frac{\int_{q_0}^{q_1} C(q) dq}{\int_{q_0}^{q_1} C_r(q) dq} \quad (23)$$

In Figure 10a we show θ as a function of the contact area fraction a/λ (notably, λ is the full contact area value) for both the frictional coupled contact condition and the frictionless uncoupled one. Of course, in both cases, for $a/\lambda \rightarrow 1$ the value of θ tends to unity, as, regardless of the degree of coupling, the coating displacements completely match the rigid rough profile. However, for $a/\lambda < 1$, the deformed interface shows higher degree of matching with the rigid profile in the presence of *geometric* coupling, as witnessed by the significantly higher values of θ , compared to the case of frictionless uncoupled interfaces. Although the contact spots can be differently located in each case, the comparison of Fig. 10a is performed at given total contact length thus the difference in θ has to be mostly ascribed to the non-contact region, where the displacements of the deformable coating appear very different

from one case to the other. This can be further investigated by looking at the contact mean separation

$$s = \frac{1}{\lambda} \int_{\lambda} g(x) dx = \Lambda - \Delta$$

where $g(x) = r(x) - [u(x) + \Delta - \Lambda]$ is the gap function, which is null within the contact domain Ω . Indeed, in Fig. 10b we plot the dimensionless normal separation \tilde{s} against a/λ , showing that larger deformations are expected out of the contact in the case of frictional coupled contacts compared to the frictionless uncoupled case. In the same figure, also the contact stiffness $K_2 = dp_m/d\Delta$ is shown indicating that the additional normal deformation introduced by the coupling term G_{21} in Eq. (2) leads to different results, depending on the contact area size. Indeed, for the case under investigation, for a contact area length up to 60% of the full contact length λ (i.e. in most of the practical applications) the frictional coupled case present lower contact stiffness compared to the frictionless uncoupled one. Only at very large contact area the scenario is reversed.

IV. CONCLUSIONS

In this work we have investigated the frictional behavior of thin soft coatings bonded to stiffer substrates in sliding rough contacts. The analysis aims at exploring the effect of the peculiar coupling between the normal and tangential displacement fields arising in the case of thin bodies. Basic Coulomb friction interactions are taken into account in the contact, so that the tangential stress distribution at the interface is non-null, and the geometric coupling can impact the system behavior. Similarly, the case of frictionless contacts is also shown for comparison, representing the uncoupled system behavior.

We found that due to coupling, also elastic rough contacts may experience keying friction depending on the coating thickness and Poisson's ratio, although no bulk dissipation occurs. A similar effect is observed also in the case of viscoelastic materials dealing, this time leading to even higher viscoelastic keying friction compared to uncoupled conditions with corresponding higher bulk energy dissipation. As a consequence, since real contacts are more likely affected by interfacial friction, faster bulk warming can be expected, with peculiar application, for instance, to tire frictional performance.

In terms of viscoelastic contact mechanics, we found that the main effect of the *geometric* coupling is to introduce additional large scale normal displacement, compared to the uncoupled case at given normal load. This leads to several peculiarities in the contact behavior of the interface under coupled conditions. The most important of them is that the contact area turns out significantly larger, compared to the uncoupled case. This entails, at moderately low normal loads, a more compliant contact behavior.

These results show that, in the case of contact interfaces involving thin deformable coatings bonded to significantly stiffer substrates, neglecting the effect of interfacial shear stresses (not necessarily related to friction) may lead to significant underestimation of both the frictional and contact behavior of the interface.

Acknowledgement 1 *This project has received funding from the European Union's Horizon 2020 research and innovation programme under the Marie Skłodowska-Curie grant agreement no. 845756 (N.M. Individual Fellowship). D.D. acknowledges the support received from the Engineering and Physical Science Research Council (EPSRC) through his Established Career Fellowship EP/N025954/1. This work was partly supported by the Italian*

- [1] Dahotre, N. B., & Nayak, S. (2005). Nanocoatings for engine application. *Surface and Coatings Technology*, 194(1), 58-67.
- [2] Kano, M. (2006). Super low friction of DLC applied to engine cam follower lubricated with ester-containing oil. *Tribology International*, 39(12), 1682-1685.
- [3] Voigt, D., Karguth, A., & Gorb, S. (2012). Shoe soles for the gripping robot: Searching for polymer-based materials maximising friction. *Robotics and Autonomous Systems*, 60(8), 1046-1055.
- [4] Greenwood, J. A., & Williamson, J. P. (1966). Contact of nominally flat surfaces. *Proc. R. Soc. Lond. A*, 295(1442), 300-319.
- [5] Bush, A.W., Gibson, R.D., Thomas, T.R., TheElastic Contact of a Rough Surface, *Wear* 1975;35:87-111.
- [6] Persson B.N.J., Theory of rubber friction and contact mechanics, *Journal of Chemical Physics* 2001;115:3840 -3861.
- [7] Yang, C. and Persson, B.N.J., Molecular Dynamics Study of Contact Mechanics: Contact Area and Interfacial Separation from Small to Full Contact, *Phys. Rev. Lett.* 2008;100.
- [8] Menga, N., Putignano, C., Carbone, G., & Demelio, G. P. (2014). The sliding contact of a rigid wavy surface with a viscoelastic half-space. *Proc. R. Soc. A*, 470(2169), 20140392.
- [9] Menga, N., Carbone, G., & Dini, D. Do uniform tangential interfacial stresses enhance adhesion? *Journal of the Mechanics and Physics of Solids* 2018;112:145-156.
- [10] Menga, N., Carbone, G., & Dini, D. (2019). WITHDRAWN: Corrigendum to: “Do uniform tangential interfacial stresses enhance adhesion?”. *Journal of the Mechanics and Physics of Solids* 2019;133:103744.
- [11] Menga, N., & Carbone, G. (2019). The surface displacements of an elastic half-space subjected to uniform tangential tractions applied on a circular area. *European Journal of Mechanics-A/Solids*, 73, 137-143.
- [12] Hyun, S., Pei, L., Molinari, J.-F., Robbins, M.O., Finite-element analysis of contact between elastic self-affine surfaces, *Phys. Rev. E* 2004;70.
- [13] Campana C., Mueser M.H. and Robbins M.O., Elastic contact between self-affine surfaces: comparison of numerical stress and contact correlation functions with analytic predictions. *J. Phys. Condens. Matter* 2008;20(35).
- [14] Pastewka, L., & Robbins, M. O. Contact area of rough spheres: Large scale simulations and simple scaling laws. *Applied Physics Letters* 2016;108(22):221601.
- [15] Medina S. and Dini D., A numerical model for the deterministic analysis of adhesive rough contacts down to the nano-scale. *International Journal of Solids and Structures* 2014;51(14):2620-2632.
- [16] Müser, M. H., Dapp, W. B., Bugnicourt, R., Sainsot, P., Lesaffre, N., Lubrecht, T. A., ... & Rohde, S. (2017). Meeting the contact-mechanics challenge. *Tribology Letters*, 65(4), 118.
- [17] Menga, N., Afferrante, L., Pugno, N. M., & Carbone, G. (2018). The multiple V-shaped double peeling of elastic thin films from elastic soft substrates. *Journal of the Mechanics and Physics*

- of Solids, 113, 56-64.
- [18] Homola, A. M., Israelachvili, J. N., McGuiggan, P. M., & Gee, M. L. (1990). Fundamental experimental studies in tribology: the transition from “interfacial” friction of undamaged molecularly smooth surfaces to “normal” friction with wear. *Wear*, 136(1), 65-83.
 - [19] Chateauminos, A., & Fretigny, C. (2008). Local friction at a sliding interface between an elastomer and a rigid spherical probe. *The European Physical Journal E: Soft Matter and Biological Physics*, 27(2), 221-227.
 - [20] Krick, B. A., Vail, J. R., Persson, B. N., & Sawyer, W. G. (2012). Optical in situ micro tribometer for analysis of real contact area for contact mechanics, adhesion, and sliding experiments. *Tribology Letters*, 45(1), 185-194.
 - [21] Ben-David, O., Cohen, G., & Fineberg, J. (2010). The dynamics of the onset of frictional slip. *Science*, 330(6001), 211-214.
 - [22] Carbone G., Lorenz B., Persson B.N.J. and Wohlers A., Contact mechanics and rubber friction for randomly rough surfaces with anisotropic statistical properties, *The European Physical Journal E – Soft Matter*, **29** (3), 275–284, (2009).
 - [23] Menga, N., L. Afferrante, and G. Carbone. Adhesive and adhesiveless contact mechanics of elastic layers on slightly wavy rigid substrates. *International Journal of Solids and Structures* 2016;88:101-109.
 - [24] Menga, N., Afferrante, L. and Carbone, G., Effect of thickness and boundary conditions on the behavior of viscoelastic layers in sliding contact with wavy profiles, *The Journal of the Mechanics and Physics of Solids* 2016;95: 517-529.
 - [25] Menga, N., Foti, D., & Carbone, G. Viscoelastic frictional properties of rubber-layer roller bearings (RLRB) seismic isolators. *Meccanica* 2017;52(11-12):2807-2817.
 - [26] Menga, N., Dini, D., & Carbone, G. (2020). Tuning the periodic V-peeling behavior of elastic tapes applied to thin compliant substrates. *International Journal of Mechanical Sciences*, 170, 105331.
 - [27] Menga, N. (2019). Rough frictional contact of elastic thin layers: The effect of geometric coupling. *International Journal of Solids and Structures*, 164, 212-220.
 - [28] Nowell, D., Hills, D. A., & Sackfield, A. (1988). Contact of dissimilar elastic cylinders under normal and tangential loading. *Journal of the Mechanics and Physics of Solids*, 36(1), 59-75.
 - [29] Chen, W. W., & Wang, Q. J. (2008). A numerical model for the point contact of dissimilar materials considering tangential tractions. *Mechanics of Materials*, 40(11), 936-948.
 - [30] Chen, W. W., & Wang, Q. J. (2009). A numerical static friction model for spherical contacts of rough surfaces, influence of load, material, and roughness. *Journal of Tribology*, 131(2), 021402.
 - [31] Wang, Z. J., Wang, W. Z., Wang, H., Zhu, D., & Hu, Y. Z. (2010). Partial slip contact analysis on three-dimensional elastic layered half space. *Journal of Tribology*, 132(2), 021403.
 - [32] Elloumi, R., Kallel-Kamoun, I., & El-Borgi, S. (2010). A fully coupled partial slip contact problem in a graded half-plane. *Mechanics of Materials*, 42(4), 417-428.
 - [33] Bental, R. H., & Johnson, K. L. (1968). An elastic strip in plane rolling contact. *International Journal of Mechanical Sciences*, 10(8), 637-663.
 - [34] Nowell, D., & Hills, D. A. (1988). Contact problems incorporating elastic layers. *International Journal of Solids and Structures*, 24(1), 105-115.
 - [35] Jaffar, M. J. (1993). Determination of surface deformation of a bonded elastic layer indented by a rigid cylinder using the Chebyshev series method. *Wear*, 170(2), 291-294.
 - [36] Jaffar, M. J. (1997). A numerical investigation of the sinusoidal model for elastic layers in line

- contact. *International journal of mechanical sciences*, 39(5), 497-506.
- [37] Kogut, L., & Komvopoulos, K. (2003). Electrical contact resistance theory for conductive rough surfaces. *Journal of Applied Physics*, 94(5), 3153-3162.
- [38] Menga, Nicola, and Michele Ciavarella. "A Winkler solution for the axisymmetric Hertzian contact problem with wear and finite element method comparison." *The Journal of Strain Analysis for Engineering Design* 50.3 (2015): 156-162.
- [39] Carbone, G., & Mangialardi, L. (2008). Analysis of the adhesive contact of confined layers by using a Green's function approach. *Journal of the Mechanics and Physics of Solids*, 56(2), 684-706.
- [40] Menga, N., Afferrante, L., Demelio, G. P., & Carbone, G. Rough contact of sliding viscoelastic layers: numerical calculations and theoretical predictions. *Tribology International*, 2018; 122:67-75.
- [41] Maugis, D., *Contact Adhesion and Rupture of Elastic Solids*. Springer-Verlag Berlin Heidelberg, 2000.
- [42] Johnson, K. L., (1987). *Contact mechanics*. Cambridge university press.
- [43] Christensen, R., (1982). *Theory of Viscoelasticity*. Academic Press
- [44] Persson, B. N., Albohr, O., Tartaglino, U., Volokitin, A. I., & Tosatti, E. (2004). On the nature of surface roughness with application to contact mechanics, sealing, rubber friction and adhesion. *Journal of physics: Condensed matter*, 17(1), R1.